JMEPEG (2012) 21:471–480
DOI: 10.1007/s11665-011-9967-3

1059-9495/$19.00

# Case-Study Inverse Thermal Analyses of Al2198 Laser Welds

*A.D. Zervaki, G.N. Haidemenopoulos, D.P. Vriami, and S.G. Lambrakos*

*(Submitted March 23, 2011)*

**In this article, case-study inverse thermal analyses of Al2198 laser welds are presented. These analyses employ a numerical methodology, that is, in terms of analytic and numerical basis functions for inverse thermal analysis of steady-state energy deposition in plate structures. The results of the case studies presented provide parametric representations of weld temperature histories that can be adopted as input data to various types of computational procedures, such as those for prediction of solid-state phase transformations and their associated software implementations. In addition, these weld temperature histories can be used for construction of numerical basis functions that can be adopted for inverse analysis of welds corresponding to other process parameters or welding processes whose process conditions are within similar regimes.**

**Keywords** aluminum, modeling processes, welding

## 1. Introduction

In this article, case-study inverse thermal analyses of Al2198 laser welds are presented. These analyses provide a parameterization of temperature histories for prediction of properties within the heat affected zone (HAZ) of welds for the regime considered. These analyses employ a procedure that is in terms of analytic and numerical basis functions for steady state energy deposition in plate structures. The formal structure of the numerical methodology underlying this procedure follows from a specific definition of the inverse heat transfer problem, which is well posed for inverse analysis of heat deposition processes. This definition is based on the assumption of the availability of information concerning spatially distributed boundary and constraint values. The results of the case study presented provide parametric representations of weld temperature histories that can be adopted as input data to various types of computational procedures, such as those for prediction of solid-state phase transformations and their associated software implementations. In addition, these weld temperature histories can be used for construction of numerical basis functions that can be adopted for inverse analysis of welds corresponding to other process parameters or of welding processes whose process conditions are within similar regimes. The construction of temperature fields according to spatially and temporally distributed constraint conditions using linear combinations of optimal basis functions represents a highly convenient approach to inverse analysis of energy deposition processes. Basis functions can be terms of either analytic or numerical function representations, or both in linear combination.

The subject areas that are presented in this article are organized as follows: first, a brief description of the general procedure for inverse analysis of heat deposition processes; second, a description of the experimental procedure for generation of laser welds of the Aluminum alloy Al2198; third, results of inverse thermal analyses of Al2198 laser welds, which provide a quantitative parametric representation of temperature histories for these welds and for any welds associated with similar welding process conditions; fourth, a discussion concerning the use of parameterized temperature histories for prediction of weld properties and for use as numerical basis functions for calculation of temperature histories associated with welding processes, process conditions of which are within similar regimes; and finally, a conclusion based on the results.

## 2. Inverse Analysis Procedure

According to the inverse analysis approach (Ref 1-6), a parametric representation based on a physical model provides a means for the inclusion of information concerning the physical characteristics of a given energy deposition process. It follows then that for heat deposition processes involving the deposition of heat within a bounded region of finite volume, consistent parametric representations of the temperature field are given by

$$T(\hat{x},t) = T_{\mathrm{A}} + \sum_{k=1}^{N_k} w_k T_k(\hat{x},\hat{x}_k,\kappa,t) \quad \text{and} \quad T(\hat{x}_n^{\mathrm{c}},t_n^{\mathrm{c}}) = T_n^{\mathrm{c}} \tag{Eq 1}$$

where $T_k(\hat{x},\hat{x}_k,\kappa,t)$ represent effectively a complete set of basis functions for representation of the temperature field within the region bounded by the inner and outer surfaces $S_{\mathrm{i}}$ and $S_{\mathrm{o}}$, respectively. The quantity $T_{\mathrm{A}}$ is the ambient temperature of the workpiece, and the locations $\hat{x}_n^{\mathrm{c}}$ and temperature values $T_n^{\mathrm{c}}$

**A.D. Zervaki, G.N. Haidemenopoulos,** and **D.P. Vriami**, Department of Mechanical Engineering, University of Thessaly, 38334 Volos, Greece; and **S.G. Lambrakos,** Center for Computational Materials, Code 6390, Materials Science and Technology Division, Naval Research Laboratory, Washington, DC. Contact e-mail: lambrakos@anvil.nrl.navy.mil.

specify constraint conditions on the temperature field. The functions $T_k(\hat{x}, \hat{x}_k, \kappa, t)$ represent an optimal basis set of functions for the given sets of boundary conditions and material properties. The quantities $\hat{x}_k = (x_k, y_k, z_k)$, $k = 1, \ldots, N_k$, are the locations of the elemental source or boundary elements. The sum defined by Eq 1 can for certain systems specify numerical integration over discrete elements of a distribution of sources or boundary elements. Selection of an optimal set of basis functions is based on considerations of the characteristic model and data spaces (Ref 6) of heat deposition processes and subsequently isolating those regions of the model space corresponding to parameterizations that are both physically consistent and sufficiently general in terms of their mathematical representation and mapping from data to model space. Although heat deposition processes may be characterized by complex coupling between the heat source and workpiece, as well as complex geometries associated with either the workpiece or deposition process, in terms of inverse analysis the general functional forms of the temperature fields associated with all such processes are within a restricted class of functions, i.e., optimal sets of functions. Accordingly, a sufficiently optimal set of functions contains the analytic solutions to heat conduction equation for a finite set of boundary conditions (Ref 7). A parameterization based on this set is both sufficiently general and convenient relative to optimization.

The formal procedure underlying the inverse method considered here entails the adjustment of the temperature field defined over the entire spatial region of the sample volume at a given time $t$. This approach defines an optimization procedure where the temperature field spanning the spatial region of the sample volume is adopted as the quantity to be optimized. The constraint conditions are imposed on the temperature field spanning the bounded spatial domain of the workpiece by minimization of the value of the objective functions defined by

$$Z_{\mathrm{T}} = \sum_{n=1}^{N} w_n \left( T(\hat{x}_n^{\mathrm{c}}, t_n^{\mathrm{c}}) - T_n^{\mathrm{c}} \right)^2 \qquad \text{(Eq 2)}$$

where $T_n^{\mathrm{c}}$ is the target temperature for position $\hat{x}_n^{\mathrm{c}} = (x_n^{\mathrm{c}}, y_n^{\mathrm{c}}, z_n^{\mathrm{c}})$.

The input of information into the inverse model defined by Eq 1 and 2, i.e., the mapping from data to model space, is effected by: the assignment of individual constraint values to the quantities $T_n^{\mathrm{c}}$; the form of the basis functions adopted for parametric representation; and specifying the shapes of the inner and outer boundaries, $S_{\mathrm{i}}$ and $S_{\mathrm{o}}$, respectively, which bound the temperature field within a specified region of the workpiece. The constraint conditions and basis functions, i.e., $T(\hat{x}_n^{\mathrm{c}}, t_n^{\mathrm{c}}) = T_n^{\mathrm{c}}$ and $T_k(\hat{x}, \hat{x}_k, \kappa, t)$, respectively, provide for the inclusion of information that can be obtained from both laboratory and numerical experiments.

Within the context of the numerical method presented, a set of basis functions is considered effectively complete if these functions provided reasonably optimal fitting to boundary and constraint conditions. Before proceeding, it is significant to note that, in principle, the set of basis functions adopted by Eq 1 can be defined in terms of either analytic or numerical

**Table 1 Chemical composition of Al2198-T8 (wt.%)**

| Si | Fe | Cu | Mn | Mg | Cr | Zn | Zr | Li | Ag | Ti |
|---|---|---|---|---|---|---|---|---|---|---|
| 0.08 | 0.10 | 3.50 | 0.5 | 0.80 | 0.05 | 0.35 | 0.18 | 1.10 | 0.5 | … |

**Table 2 Temperature field constraint conditions at positions ($y_c$, $z_c$) on transverse cross sections of welds at solidification boundaries**

| Power $P$ | 3441 W | 3441 W | 3441 W | 2970 W | 3913 W | 3252 W | 3441 W | 3630 W | 3252 W | 3252 W |
|---|---|---|---|---|---|---|---|---|---|---|
| Speed $V$ | 2 m/min | 2 m/min | 2 m/min | 2 m/min | 2 m/min | 2 m/min | 2 m/min | 2 m/min | 1.8 m/min | 1.6 m/min |
| Input $h$ | 103 J/mm | 103 J/mm | 103 J/mm | 89 J/mm | 117 J/mm | 98 J/mm | 103 J/mm | 109 J/mm | 108 J/mm | 122 J/mm |
| Focal point | 1 mm | −1 mm | 0 mm | 0 mm | 0 mm | 0 mm | 0 mm | 0 mm | 0 mm | 0 mm |
| $z_c$, mm | $2y_c$, mm | $2y_c$, mm | $2y_c$, mm | $2y_c$, mm | $2y_c$, mm | $2y_c$, mm | $2y_c$, mm | $2y_c$, mm | $2y_c$, mm | $2y_c$, mm |
| 0.0 | 4.25 | 4.0 | 4.375 | 4.125 | 4.0 | 4.75 | 4.0 | 4.5 | 4.375 | 4.25 | 4.5 |
| 0.5 | 3.875 | 3.875 | 4.25 | 4.0 | 3.75 | | | | 4.5 | 4.2 | |
| 0.75 | | | | | | 4.5 | | | | | |
| 1.0 | 3.25 | 3.5 | 3.75 | 3.375 | | | 3.25 | 3.875 | 4.0 | 3.75 | 4.5 |
| 1.5 | 2.125 | 2.75 | 2.75 | 2.5 | 2.5 | 3.4 | | | 3.125 | 2.875 | |
| 1.75 | | | | | | | | 2.625 | | | |
| 2.0 | 1.875 | 2.175 | 2.375 | 2.125 | 2.25 | | 2.125 | 2.375 | 2.25 | 2.3 | 3.8 |
| 2.5 | 1.625 | 1.875 | 2.125 | 1.875 | 1.75 | 3.0 | | | 2.0 | 2.25 | |
| 3.0 | 1.5 | 1.75 | 1.875 | 1.75 | 3.0 | 3.0 | 1.75 | 2.5 | 2.375 | 2.0 | 3.5 |
| 3.33 | | | | | 0.0 | | | | | | |
| 3.5 | | | 2.0 | 1.625 | | | | | | 1.875 | |
| 3.8 | 1.5 | 1.875 | 2.125 | 1.875 | | 3.25 | 1.625 | 2.75 | 2.5 | 2.25 | 4.2 |
| Figure | 1 | 2 | 3 | 4(a) | 4(b) | 4(c) | 4(d) | 4(e) | 4(f) | 4(g) | 4(h) |

**Table 3 Volumetric source function $C(\hat{x}_k)$ calculated according to constraint conditions specified by weld cross sections shown in Fig. 1, where $\Delta l$ = 3.8/60 mm**

| $k$ | $C(\hat{x}_k)$/2.9 | $x_k(\Delta l)$ | $y_k(\Delta l)$ | $z_k(\Delta l)$ |
|---|---|---|---|---|
| 1 | 0.042 | 0.0 | 0.0 | 3.0 |
| 2 | 0.041 | 0.0 | 0.0 | 5.0 |
| 3 | 0.038 | 0.0 | 0.0 | 7.0 |
| 4 | 0.03 | 0.0 | 0.0 | 9.0 |
| 5 | 0.03 | 0.0 | 0.0 | 11.0 |
| 6 | 0.03 | 0.0 | 0.0 | 13.0 |
| | $C(\hat{x}_k)$/1.3 | $x_k(\Delta l)$ | $y_k(\Delta l)$ | $z_k(\Delta l)$ |
| 7 | 0.1 | 4.0 | 0.0 | 0.0 |
| 8 | 0.1 | −4.0 | 0.0 | 0.0 |
| 9 | 0.1 | 0.0 | 4.0 | 0.0 |
| 10 | 0.1 | 0.0 | −4.0 | 0.0 |

**Table 4 Volumetric source function $C(\hat{x}_k)$ calculated according to constraint conditions specified by weld cross sections shown in Fig. 2, where $\Delta l$ = 3.8/60**

| $k$ | $C(\hat{x}_k)$/2.9 | $x_k(\Delta l)$ | $y_k(\Delta l)$ | $z_k(\Delta l)$ |
|---|---|---|---|---|
| 1 | 0.015 | 0.0 | 0.0 | 3.0 |
| 2 | 0.015 | 0.0 | 0.0 | 5.0 |
| 3 | 0.025 | 0.0 | 0.0 | 7.0 |
| 4 | 0.027 | 0.0 | 0.0 | 9.0 |
| 5 | 0.027 | 0.0 | 0.0 | 11.0 |
| 6 | 0.025 | 0.0 | 0.0 | 13.0 |
| | $C(\hat{x}_k)$/1.3 | $x_k(\Delta l)$ | $y_k(\Delta l)$ | $z_k(\Delta l)$ |
| 7 | 0.1 | 4.0 | 0.0 | 0.0 |
| 8 | 0.1 | −4.0 | 0.0 | 0.0 |
| 9 | 0.1 | 0.0 | 4.0 | 0.0 |
| 10 | 0.1 | 0.0 | −4.0 | 0.0 |

**Table 5 Volumetric source function $C(\hat{x}_k)$ calculated according to constraint conditions specified by weld cross sections shown in Fig. 3, where $\Delta l$ = 3.8/60 mm**

| $k$ | $C(\hat{x}_k)$/2.9 | $x_k$ ($\Delta l$) | $y_k$ ($\Delta l$) | $z_k$ ($\Delta l$) |
|---|---|---|---|---|
| 1 | 0.05 | 0.0 | 0.0 | 3.0 |
| 2 | 0.045 | 0.0 | 0.0 | 5.0 |
| 3 | 0.045 | 0.0 | 0.0 | 7.0 |
| 4 | 0.027 | 0.0 | 0.0 | 9.0 |
| 5 | 0.027 | 0.0 | 0.0 | 11.0 |
| 6 | 0.025 | 0.0 | 0.0 | 13.0 |
| | $C(\hat{x}_k)$/1.3 | $x_k(\Delta l)$ | $y_k(\Delta l)$ | $z_k(\Delta l)$ |
| 7 | 0.1 | 4.0 | 0.0 | 0.0 |
| 8 | 0.1 | −4.0 | 0.0 | 0.0 |
| | $C(\hat{x}_k)$/0.9 | $x_k(\Delta l)$ | $y_k(\Delta l)$ | $z_k(\Delta l)$ |
| 9 | 0.1 | 0.0 | 4.0 | 0.0 |
| 10 | 0.1 | 0.0 | −4.0 | |

**Table 6 Volumetric source function $C(\hat{x}_k)$ calculated according to constraint conditions specified by weld cross sections shown in Fig. 4(a), where $\Delta l$ = 3.8/60 mm**

| $k$ | $C(\hat{x}_k)$/2.7 | $x_k(\Delta l)$ | $y_k(\Delta l)$ | $z_k(\Delta l)$ |
|---|---|---|---|---|
| 1 | 0.05 | 0.0 | 0.0 | 3.0 |
| 2 | 0.045 | 0.0 | 0.0 | 5.0 |
| 3 | 0.045 | 0.0 | 0.0 | 7.0 |
| 4 | 0.027 | 0.0 | 0.0 | 9.0 |
| 5 | 0.027 | 0.0 | 0.0 | 11.0 |
| 6 | 0.025 | 0.0 | 0.0 | 13.0 |
| | $C(\hat{x}_k)$/1.3 | $x_k(\Delta l)$ | $y_k(\Delta l)$ | $z_k(\Delta l)$ |
| 7 | 0.1 | 4.0 | 0.0 | 0.0 |
| 8 | 0.1 | −4.0 | 0.0 | 0.0 |
| | $C(\hat{x}_k)$/0.9 | $x_k(\Delta l)$ | $y_k(\Delta l)$ | $z_k(\Delta l)$ |
| 9 | 0.1 | 0.0 | 4.0 | 0.0 |
| 10 | 0.1 | 0.0 | −4.0 | |

**Table 7 Volumetric source function $C(\hat{x}_k)$ calculated according to constraint conditions specified by weld cross sections shown in Fig. 4(b), where $\Delta l$ = 3.8/60 mm**

| $k$ | $C(\hat{x}_k)$/2.7 | $x_k(\Delta l)$ | $y_k(\Delta l)$ | $z_k(\Delta l)$ |
|---|---|---|---|---|
| 1 | 0.05 | 0.0 | 0.0 | 3.0 |
| 2 | 0.045 | 0.0 | 0.0 | 5.0 |
| 3 | 0.045 | 0.0 | 0.0 | 7.0 |
| 4 | 0.031 | 0.0 | 0.0 | 9.0 |
| 5 | 0.01 | 0.0 | 0.0 | 10.0 |
| | $C(\hat{x}_k)$/1.3 | $x_k(\Delta l)$ | $y_k(\Delta l)$ | $z_k(\Delta l)$ |
| 6 | 0.1 | 4.0 | 0.0 | 0.0 |
| 7 | 0.1 | −4.0 | 0.0 | 0.0 |
| | $C(\hat{x}_k)$/0.9 | $x_k(\Delta l)$ | $y_k(\Delta l)$ | $z_k(\Delta l)$ |
| 8 | 0.1 | 0.0 | 4.0 | 0.0 |
| 9 | 0.1 | 0.0 | −4.0 | |

**Table 8 Volumetric source function $C(\hat{x}_k)$ calculated according to constraint conditions specified by weld cross sections shown in Fig. 4(c), where $\Delta l$ = 3.8/60 mm**

| $k$ | $C(\hat{x}_k)$/4.4 | $x_k(\Delta l)$ | $y_k(\Delta l)$ | $z_k(\Delta l)$ |
|---|---|---|---|---|
| 1 | 0.05 | 0.0 | 0.0 | 3.0 |
| 2 | 0.045 | 0.0 | 0.0 | 5.0 |
| 3 | 0.045 | 0.0 | 0.0 | 7.0 |
| 4 | 0.041 | 0.0 | 0.0 | 9.0 |
| 5 | 0.01 | 0.0 | 0.0 | 11.0 |
| 6 | 0.07 | 0.0 | 0.0 | 13.0 |
| | $C(\hat{x}_k)$/1.3 | $x_k(\Delta l)$ | $y_k(\Delta l)$ | $z_k(\Delta l)$ |
| 7 | 0.1 | 4.0 | 0.0 | 0.0 |
| 8 | 0.1 | −4.0 | 0.0 | 0.0 |
| 9 | 0.1 | 0.0 | 4.0 | 0.0 |
| 10 | 0.1 | 0.0 | −4.0 | |

**Table 9 Volumetric source function $C(\hat{x}_k)$ calculated according to constraint conditions specified by weld cross sections shown in Fig. 4(d), where $\Delta l$ = 3.8/60 mm**

| $k$ | $C(\hat{x}_k)$/2.4 | $x_k(\Delta l)$ | $y_k(\Delta l)$ | $z_k(\Delta l)$ |
|---|---|---|---|---|
| 1 | 0.05 | 0.0 | 0.0 | 3.0 |
| 2 | 0.045 | 0.0 | 0.0 | 5.0 |
| 3 | 0.045 | 0.0 | 0.0 | 7.0 |
| 4 | 0.041 | 0.0 | 0.0 | 9.0 |
| 5 | 0.012 | 0.0 | 0.0 | 11.0 |
| 6 | 0.038 | 0.0 | 0.0 | 13.0 |
| | $C(\hat{x}_k)$/1.3 | $x_k(\Delta l)$ | $y_k(\Delta l)$ | $z_k(\Delta l)$ |
| 7 | 0.1 | 4.0 | 0.0 | 0.0 |
| 8 | 0.1 | −4.0 | 0.0 | 0.0 |
| | $C(\hat{x}_k)$/1.0 | $x_k(\Delta l)$ | $y_k(\Delta l)$ | $z_k(\Delta l)$ |
| 9 | 0.1 | 0.0 | 4.0 | 0.0 |
| 10 | 0.1 | 0.0 | −4.0 | |

**Table 10 Volumetric source function $C(\hat{x}_k)$ calculated according to constraint conditions specified by weld cross sections shown in Fig. 4(e), where $\Delta l$ = 3.8/60 mm**

| $k$ | $C(\hat{x}_k)$/2.3 | $x_k(\Delta l)$ | $y_k(\Delta l)$ | $z_k(\Delta l)$ |
|---|---|---|---|---|
| 1 | 0.05 | 0.0 | 0.0 | 3.0 |
| 2 | 0.045 | 0.0 | 0.0 | 5.0 |
| 3 | 0.045 | 0.0 | 0.0 | 7.0 |
| 4 | 0.041 | 0.0 | 0.0 | 9.0 |
| 5 | 0.042 | 0.0 | 0.0 | 11.0 |
| 6 | 0.087 | 0.0 | 0.0 | 13.0 |
| | $C(\hat{x}_k)$/1.3 | $x_k(\Delta l)$ | $y_k(\Delta l)$ | $z_k(\Delta l)$ |
| 7 | 0.1 | 4.0 | 0.0 | 0.0 |
| 8 | 0.1 | −4.0 | 0.0 | 0.0 |
| | $C(\hat{x}_k)$/1.5 | $x_k(\Delta l)$ | $y_k(\Delta l)$ | $z_k(\Delta l)$ |
| 9 | 0.1 | 0.0 | 4.0 | 0.0 |
| 10 | 0.1 | 0.0 | −4.0 | |

function representations. The numerical method that is developed here employs both analytic and numerical function representations of basis functions, which are to be adopted for the calculation of temperature fields within bounded domains for which constraint conditions are specified. Finally, the interrelation between analytic and numerical basis function representations is an important aspect of the numerical method applied in this analysis, which underlies its flexibility for convenient inverse analysis.

It follows then that a consistent representation Eq 1 of the temperature field for heat deposition within structures characterized by a finite thickness, in terms of analytic basis functions, i.e., analytic solutions to the heat conduction equation (Ref 7), is

$$T(\hat{x},t) = T_{\mathrm{A}} + \sum_{k=1}^{N_k}\sum_{n=1}^{N_t} C(\hat{x}_k)G(\hat{x},\hat{x}_k,\kappa,n\Delta t,V) \quad \text{and} \quad T(\hat{x}_n^{\mathrm{c}},t_n^{\mathrm{c}}) = T_n^{\mathrm{c}}, \qquad \text{(Eq 3)}$$

where

**Table 11 Volumetric source function $C(\hat{x}_k)$ calculated according to constraint conditions specified by weld cross sections shown in Fig. 4(f), where $\Delta l$ = 3.8/60 mm**

| $k$ | $C(\hat{x}_k)$/2.3 | $x_k(\Delta l)$ | $y_k(\Delta l)$ | $z_k(\Delta l)$ |
|---|---|---|---|---|
| 1 | 0.07 | 0.0 | 0.0 | 3.0 |
| 2 | 0.055 | 0.0 | 0.0 | 5.0 |
| 3 | 0.04 | 0.0 | 0.0 | 7.0 |
| 4 | 0.02 | 0.0 | 0.0 | 9.0 |
| 5 | 0.03 | 0.0 | 0.0 | 11.0 |
| 6 | 0.087 | 0.0 | 0.0 | 13.0 |
| | $C(\hat{x}_k)$/1.3 | $x_k(\Delta l)$ | $y_k(\Delta l)$ | $z_k(\Delta l)$ |
| 7 | 0.1 | 4.0 | 0.0 | 0.0 |
| 8 | 0.1 | −4.0 | 0.0 | 0.0 |
| | $C(\hat{x}_k)$/1.5 | $x_k(\Delta l)$ | $y_k(\Delta l)$ | $z_k(\Delta l)$ |
| 9 | 0.1 | 0.0 | 4.0 | 0.0 |
| 10 | 0.1 | 0.0 | −4.0 | |

**Table 12 Volumetric source function $C(\hat{x}_k)$ calculated according to constraint conditions specified by weld cross sections shown in Fig. 4(g), where $\Delta l$ = 3.8/60 mm**

| $k$ | $C(\hat{x}_k)$/2.3 | $x_k(\Delta l)$ | $y_k(\Delta l)$ | $z_k(\Delta l)$ |
|---|---|---|---|---|
| 1 | 0.07 | 0.0 | 0.0 | 3.0 |
| 2 | 0.055 | 0.0 | 0.0 | 5.0 |
| 3 | 0.04 | 0.0 | 0.0 | 7.0 |
| 4 | 0.04 | 0.0 | 0.0 | 9.0 |
| 5 | 0.04 | 0.0 | 0.0 | 11.0 |
| 6 | 0.038 | 0.0 | 0.0 | 13.0 |
| | $C(\hat{x}_k)$/1.3 | $x_k(\Delta l)$ | $y_k(\Delta l)$ | $z_k(\Delta l)$ |
| 7 | 0.1 | 4.0 | 0.0 | 0.0 |
| 8 | 0.1 | −4.0 | 0.0 | 0.0 |
| 9 | 0.1 | 0.0 | 4.0 | 0.0 |
| 10 | 0.1 | 0.0 | −4.0 | 0.0 |

**Table 13 Volumetric source function $C(\hat{x}_k)$ calculated according to constraint conditions specified by weld cross sections shown in Fig. 4(h), where $\Delta l$ = 3.8/60 mm**

| $k$ | $C(\hat{x}_k)$/2.3 | $x_k(\Delta l)$ | $y_k(\Delta l)$ | $z_k(\Delta l)$ |
|---|---|---|---|---|
| 1 | 0.09 | 0.0 | 0.0 | 3.0 |
| 2 | 0.085 | 0.0 | 0.0 | 5.0 |
| 3 | 0.08 | 0.0 | 0.0 | 7.0 |
| 4 | 0.08 | 0.0 | 0.0 | 9.0 |
| 5 | 0.015 | 0.0 | 0.0 | 10.0 |
| 6 | 0.015 | 0.0 | 0.0 | 11.0 |
| 7 | 0.24 | 0.0 | 0.0 | 13.0 |
| | $C(\hat{x}_k)$/1.3 | $x_k(\Delta l)$ | $y_k(\Delta l)$ | $z_k(\Delta l)$ |
| 8 | 0.1 | 4.0 | 0.0 | 0.0 |
| 9 | 0.1 | −4.0 | 0.0 | 0.0 |
| 10 | 0.1 | 0.0 | 4.0 | 0.0 |
| 11 | 0.1 | 0.0 | −4.0 | 0.0 |

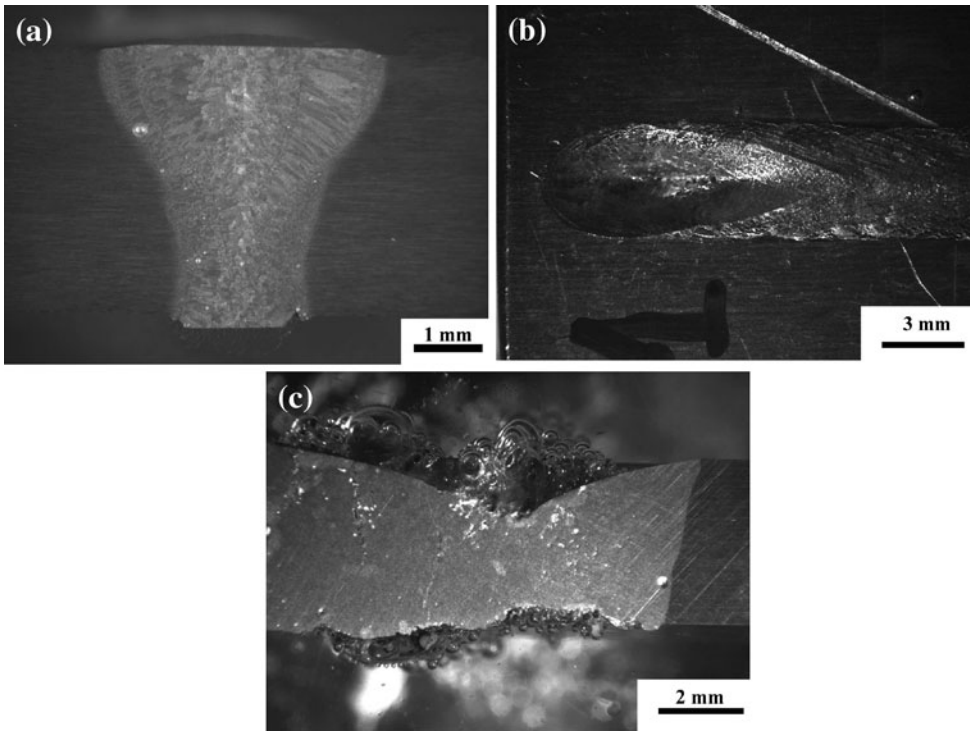


**Fig. 1** Laser beam weld of Al2198-T8 for energy deposition of 103 J/mm and beam focal point at 1 mm above top surface of workpiece. (a) Transverse cross section. (b) Top surface of workpiece. (c) Longitudinal cross section at symmetry plane. Beam power and welding speed are 3441 W and 2 m/min, respectively

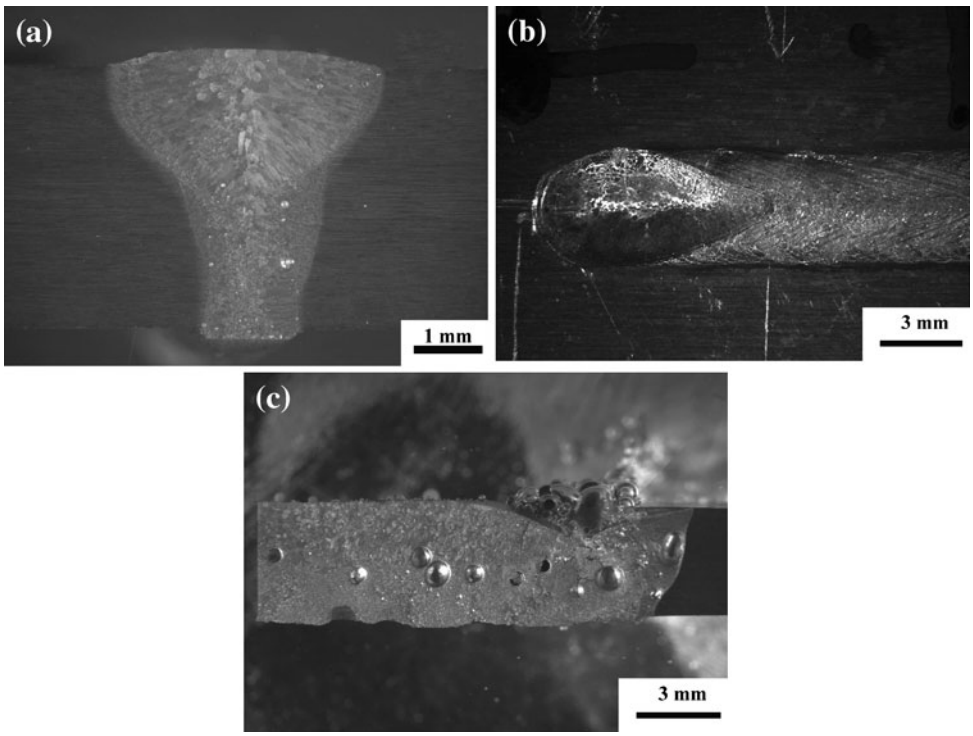


**Fig. 2** Laser beam weld of Al2198-T8 for energy deposition of 103 J/mm and beam focal point at 1 mm below top surface of workpiece. (a) Transverse cross section. (b) Top surface of workpiece. (c) Longitudinal cross section at symmetry plane. Beam power and welding speed are 3441 W and 2 m/min, respectively

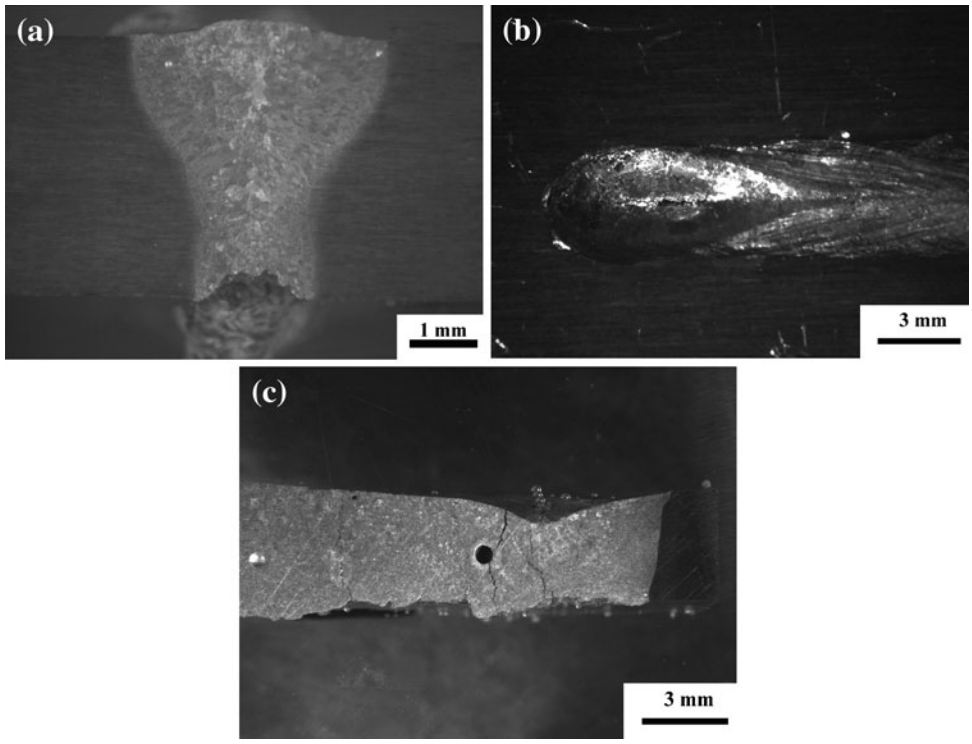


**Fig. 3** Laser beam weld of Al2198-T8 for energy deposition of 103 J/mm and beam focal point at top surface of workpiece. (a) Transverse cross section. (b) Top surface of workpiece. (c) Longitudinal cross section at symmetry plane. Beam power and welding speed are 3441 W and 2 m/min, respectively

$$G(\hat{x}, \hat{x}_k, t, \kappa, V) = \frac{1}{t}\exp\left[-\frac{(x - x_k - Vt)^2 + (y - y_k)^2}{4\kappa t}\right] \times \left\{1 + 2\sum_{m=1}^{\infty}\exp\left[-\frac{\kappa m^2\pi^2 t}{l^2}\right]\cos\left[\frac{m\pi z}{l}\right]\cos\left[\frac{m\pi z_k}{l}\right]\right\}, \quad \text{(Eq 4)}$$

and

$$C(\hat{x}) = \sum_{k=1}^{N_k} Q(\hat{x}_k)\delta(\hat{x} - \hat{x}_k). \quad \text{(Eq 5)}$$

The quantities κ, $V$, and $l$ are the thermal diffusivity, welding speed, and plate thickness, respectively. The procedure for inverse analysis defined by Eq 2-5 entails adjustment of the parameters $C(\hat{x}_k)$, $\hat{x}_k$ and $\Delta t$ defined over the entire spatial region of the workpiece.

## 3. Experimental Procedure

The heat-treatable aluminum alloy used for this study is the Al-alloy 2198-T8, with plate dimensions, 100 × 100 × 3.8 mm. Chemical composition of this alloy (in wt.%) is given in Table 1.

A Trumpf TLF 12000 $CO_2$ laser was employed for the welding experiments. The lens of the welding head had a focal distance of 171.5 mm and the beam spot size at the focal point position was 0.6 mm. Shielding gas (50:50 mixture of Ar and He) was supplied coaxially to the laser beam for plasma suppression during keyhole formation to avoid loss of alloying elements, especially magnesium, from vaporization. Bead-on-plate experiments were conducted and the welding conditions, including laser travel speed and focal point position, are given in Table 2. In these tables, laser welding conditions of power $P$ (W) and travel speed $V$ (m/min) are represented by the heat input parameter ($h$) which is defined by $h = P/V$ (J/mm). Specimens for metallographic evaluation were cut from the welded plates in longitudinal and transverse directions to the weld bead direction. Standard metallographic specimen preparation was employed including grinding, polishing, and etching. The etchant for macrostructure was a mixture of HCl, $HNO_3$, HF, and $H_2O$. For revealing microstructure, Keller's reagent was used.

## 4. Case Study Analysis of Al2198 Laser Welds

The procedure for construction of numerical basis functions adopted in this case study entails calculation of the steady-state temperature field for a specified range of sizes and shapes of the inner surface boundary $S_i$ defined by the solidification boundary for a range of welding process parameters. For this system, the parameter values assumed are $\kappa = 1.88 \times 10^{-5}$ $m^2/s$, $T_M$ = 567 °C (solidus temperature of 2198-T8 Aluminum) and $l$ = 3.8 mm. The upstream boundary constraints on the temperature field, $T_c = T_M$ for ($y_c$, $z_c$) defined in Eq 3, are given in Table 1. Given in Tables 3-13 are the values of the discrete source function that have been calculated according to the constraint conditions and weld process parameters given in Table 1.

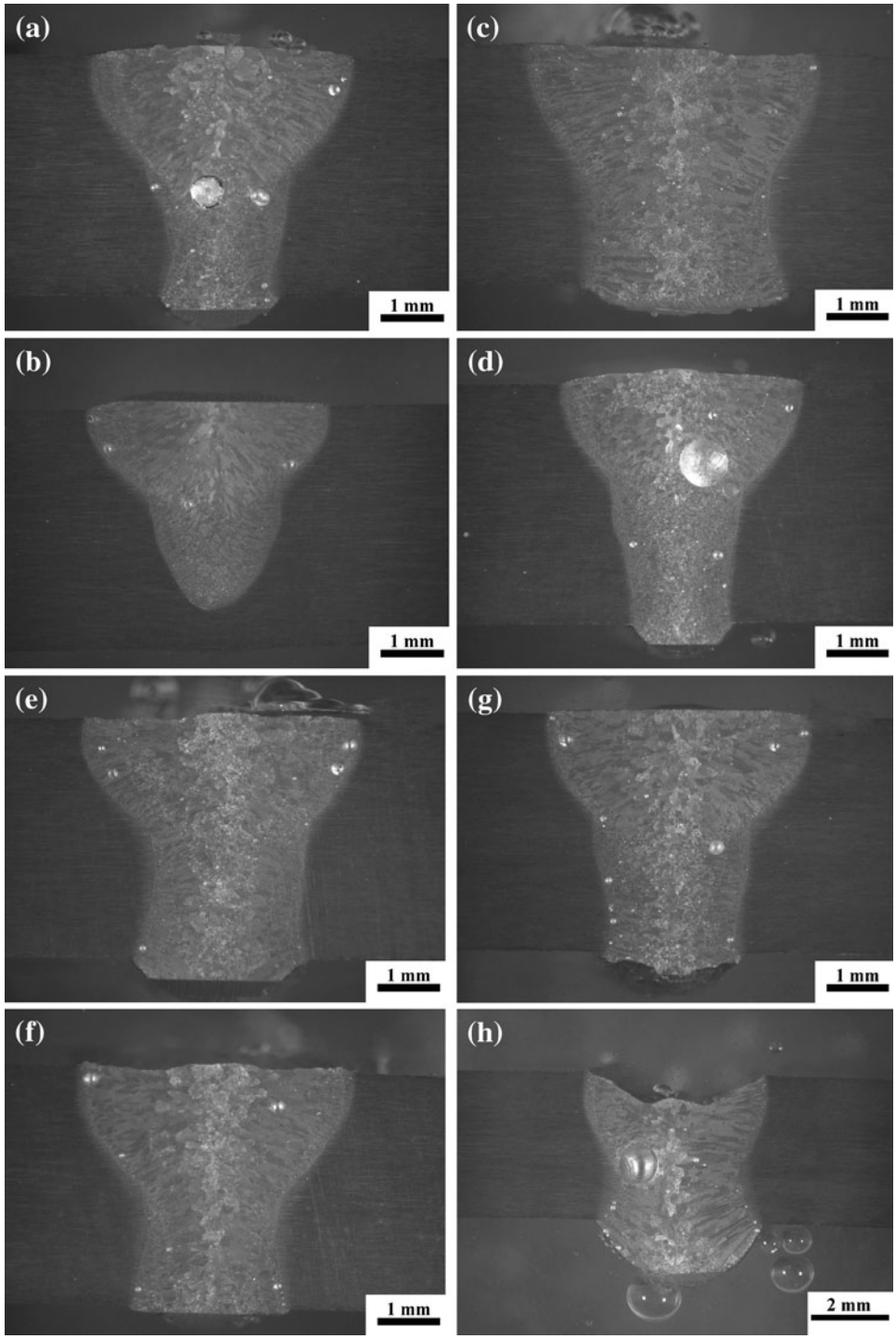


**Fig. 4** Transverse cross sections of laser beam welds of Al2198-T8 corresponding to different process parameters (see Table 1)

## 5. Procedure for Calculation of Temperature Histories

The discussion presented in this section concerning weld analysis using numerical basis functions represents a brief summary of the procudure for calculating temeperature histories using the parameters given above. Proceeding further, Tables 3-13 provide a representation of the temperature field for the welding processes considered in this study in terms of linear combinations of numerical basis functions. That is to say, Tables 3-13 specify a set of basis functions for representation of the temperature field for welding processes parameter values of which are within the associated neighborhood of parameter space. Accordingly, the procedure for calculation of temperature field values entails small adjustments of the coefficients $A_k$ defined in the expression:

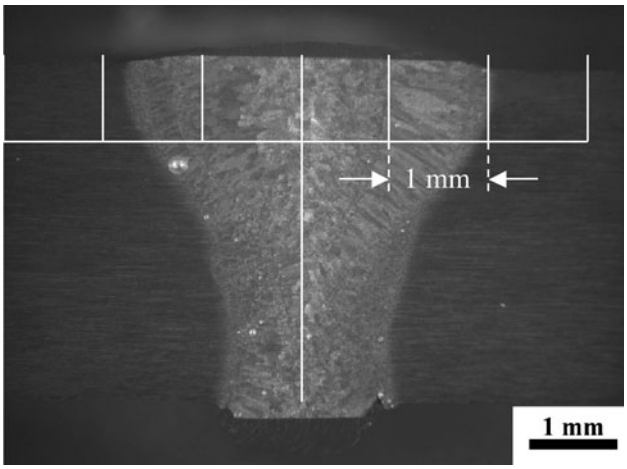


**Fig. 5** Transverse cross section of laser beam weld of Al2198-T8 shown in Fig. 1 and region of interest within HAZ for calculation of temperature histories

$$T(\hat{x},t) = T_{\mathrm{A}} + \sum_{k=1}^{N_k}\sum_{n=1}^{N_t} A_k C(\hat{x}_k) G(\hat{x},\hat{x}_k,\kappa,n\Delta t) \qquad \text{(Eq 6)}$$

where $T(\hat{x}_n^c, t_n^c) = T_n^c$, and the values of the source function $C(\hat{x}_k)$ are given in Tables 3-13 and the function $G(\hat{x},\hat{x}_k,\kappa,n\Delta t)$ is given by Eq 4. In practice, following the simplest procedure, the weld analyst would proceed as follows. First, the weld cross sections, shown in Fig. 1-4, which also represent essentially a pictorial directory for selection of initial values of the source function $C(\hat{x}_k)$, provide initial estimates of $C(\hat{x}_k)$, which are in the neighborhood of values corresponding to the target temperature field. Second, since these source function values are for a temperature field in the neighborhood of the target field, only small adjustments of the values of $C(\hat{x}_k)$ are required, which are effected via the coefficients $A_k$ defined in Eq 6. Finally, given small variations of the function $C(\hat{x}_k)$, the numerical basis functions will be sufficiently complete in the sense that temperature fields can be calculated, using the linear combination defined by Eq 6,

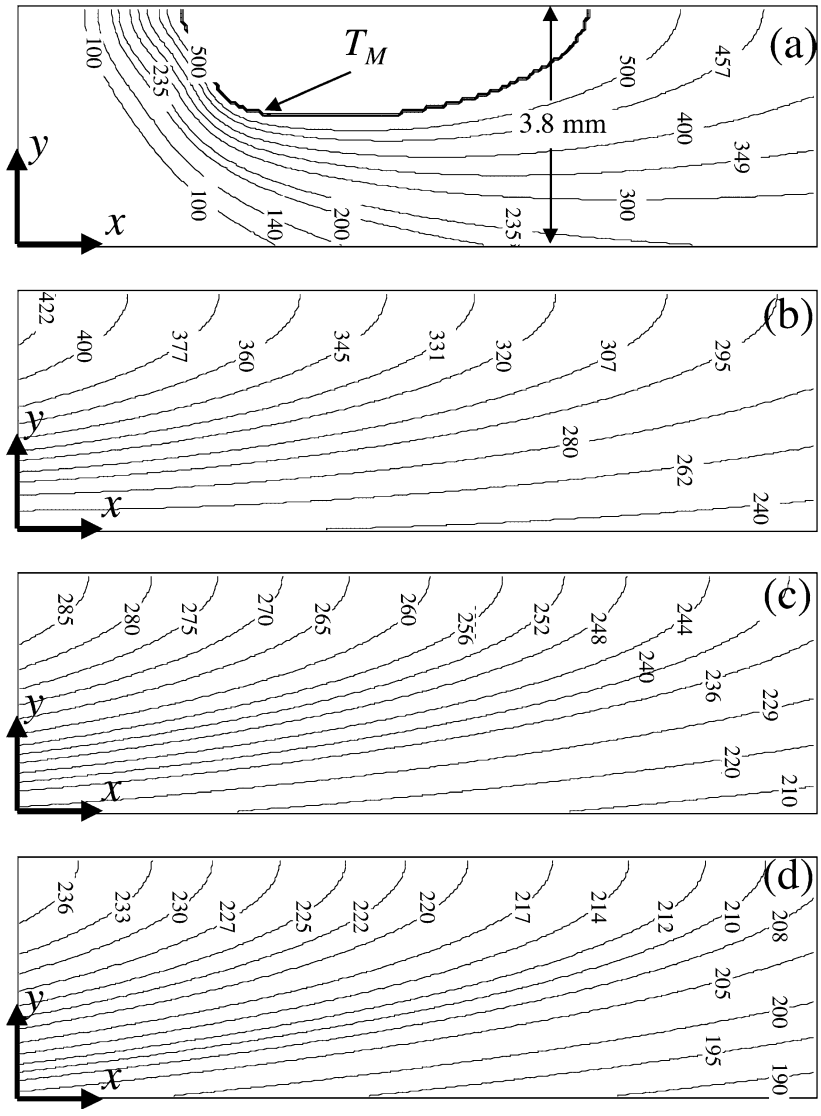


**Fig. 6** Temperature history (°C) at plane 1 mm below surface of workpiece shown in Fig. 5 expressed in terms of Galilean transformation $x = Vt$, the time periods shown are: (a) 0-0.38 s, (b) 0.38-0.76 s, (c) 0.76-1.14 s, (d) 1.14-1.52 s, (e) 3.8-4.18 s, (f) 4.94-5.32 s, (g) 6.08-6.46 s, and (h) 7.22-7.6 s

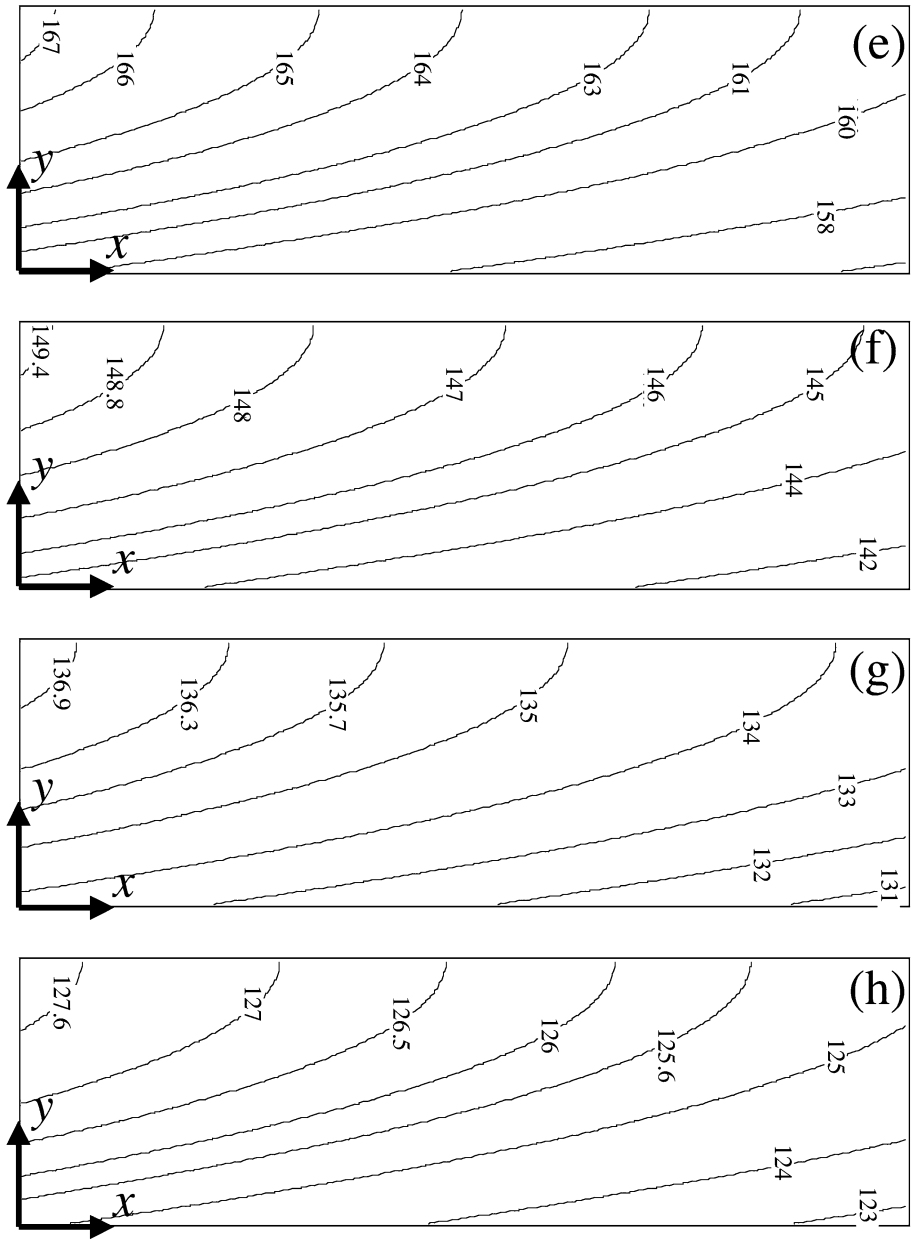


**Fig. 6** Continued

which satisfy the objective function Eq 2 for constraint values corresponding to all process parameters within a bounded set of values. This procedure can be extended to include the small variations of diffusivity κ, the sample thickness $l$, and the welding speed $V$, i.e.,

$$T(\hat{x},t) = T_{\mathrm{A}} + \sum_{k=1}^{N_k}\sum_{n=1}^{N_t} A_k C(\hat{x}_k) G(\hat{x},\hat{x}_k,B_k\kappa,C_k l,D_k V,n\Delta t) \quad \text{(Eq 7)}$$

where $T(\hat{x}_n^{\mathrm{c}},t_n^{\mathrm{c}}) = T_n^{\mathrm{c}}$, $\kappa - \Delta\kappa < B_k\kappa < \kappa + \Delta\kappa$, $l - \Delta l < C_k l < l + \Delta l$ and $V - \Delta V < D_k V < V + \Delta V$. Accordingly, if bounds on the variations of κ, $l$ and $V$, i.e., $\pm\Delta\kappa$, $\pm\Delta l$ and $\pm\Delta V$, are not sufficiently small, then it is necessary to calculate new sets of values of the source function $C(\hat{x}_k)$ for the generation of numerical basis functions which are sufficiently complete. That is, new values of $C(\hat{x}_k)$ are calculated by iterative adjustment, until Eq 2 is satisfied with respect to new sets of constraint conditions $T_n^{\mathrm{c}}$.

An example of temperature histories calculated according to the procedure described above is given with reference to Fig. 5. For this example, temperature histories within the HAZ at positions 1.0 mm below the surface of the workpiece are desired. Accordingly, by substitution of the parameter values given in Table 3 into Eq 3-5, one obtains the temperature histories shown in Fig. 6. Referring to Fig. 6, it must be noted that the $x$-coordinate is proportional to time according to the Galilean transformation $x = Vt$, which is consistent with the assumption of steady-state conditions. In practice, these temperature histories would then be adopted as input to other physical models and associated software for the prediction of solid-phase transformations. The results of such calculations

would then be correlated with experimentally observed microstructure.

## 6. Conclusion

The objective of this report is to describe a quantitative inverse thermal analysis of Al2198 laser welds corresponding to a specific range of weld process parameters and to construct numerical basis functions that can be used by weld analyst to calculate weld temperature histories, which are for welding processes associated with similar process conditions. A significant aspect of the results presented in this report are that they contribute to the continuing evolution of a multidimensional temperature field $T(\hat{x}, t, \kappa, V, l)$, which can be adopted for subsequent inverse thermal analysis by construction of numerical basis functions by interpolation within the ($\kappa$, $V$, $l$) parameter space.


### Acknowledgments

The authors (ADZ and GNH) would like to thank the German Research Foundation DFG for the support of the depicted research within the Cluster of Excellence ''Integrative Production Technology for High-Wage Countries'' at RWTH Aachen University. Also ADZ acknowledges the support of Dr. Alexander Drenker of Fraunhofer-Institut für Lasertechnik during the experimental research. One of the authors (SGL) acknowledges the support by the Naval Research Laboratory (NRL) internal core program and active scientific collaboration with the University of Thessaly.


### References


1. S.G. Lambrakos, A.D. Zervaki, G.N. Haidemenopoulos, and V. Stergiou, Basis Functions and Parameterizations for Inverse Analysis of Welding Processes, *Mathematical Modelling of Weld Phenomena*, Vol 9, Verlag der Technischen Universite Graz, Graz, 2011, p 793–815
2. A.D. Zervaki, G.N. Haidemenopoulos, and S.G. Lambrakos, Analysis of Heat Affected Zone using Direct and Inverse Modelling in 6XXX Aluminum Alloys, *Mathematical Modelling of Weld Phenomena*, Vol 8, Verlag der Technischen Universite Graz, Graz, 2007, p 907–923
3. S.G**.** Lambrakos and S.G. Michopoulos, Algorithms for Inverse Analysis of Heat Deposition Processes, *Mathematical Modelling of Weld Phenomena*, Vol 8, Published by Verlag der Technischen Universite Graz, Graz, 2007, p 847–879
4. S.G. Lambrakos and J.O. Milewski, Analysis of Welding and Heat Deposition Processes Using an Inverse-Problem Approach, *Mathematical Modelling of Weld Phenomena*, Vol 7, Verlag der Technischen Universite Graz, Graz, 2005, p 1025–1055
5. J. Xie and J. Zou, Numerical Reconstruction of Heat Fluxes, *SIAM J. Numer. Anal.*, 2005, **43**(4), p 1504–1535
6. A. Tarantola, *Inverse Problem Theory and Methods for Model Parameter Estimation*, SIAM, Philadelphia, PA, 2005
7. H.S. Carslaw and J.C. Jaegar, *Conduction of Heat in Solids*, 2nd ed., Clarendon Press, Oxford, 1959, p 374